SUPPLEMENTAL INFORMATION FOR VICTORA ET AL.

Supplemental figure legends

Figure S1. Levels of expression of photoactivatable green fluorescent protein in PA-GFP transgenic mice. Related to Figure 1.

(A) Expression of PA-GFP (405 nm excitation) in blood lymphocytes of homozygous and heterozygous PA-GFP transgenic mice.

(B) Expression of PA-GFP in splenocytes from PA-GFP+/+ or -/- mice. Gated on live/single/single/CD45+ cells.

(C) Expression of PA-GFP in different splenocyte populations from PA-GFP+/+ or -/- mice. Gated as follows: B cells, $CD45^{+}CD19^{+}CD3^{-}$; T cells, $CD45^{+}CD3^{+}CD19^{-}$; NK cells, $CD45^{+}CD3^{-}NK1.1^{+}$; DCs, $CD45^{+}CD3/19^{-}CD11c^{hi}CD11b^{int}$; monocytes/macrophages, $CD45^{+}CD3/19/11c^{-}CD11b^{hi}SSC^{lo}$; granulocytes, $CD45^{+}CD3/19/11c^{-}CD11b^{hi}SSC^{hi}$. gMFI = geometric mean fluorescence intensity (arbitrary units). SSC = side scatter.

(D) Decay in PA-GFP fluorescence after activation. Data from two independent experiments are plotted as a percentage of the initial *ex vivo* fluorescence under 488 nm excitation after background subtraction. Data plotted are mean and range. Half-life was calculated using the *one phase exponential decay* function in Prism software v. 5.0.

Figure S2. Expression of selected surface markers by light and dark zone

GC cells. Related to Figure 2.

(A) PA-GFP cells were photoactivated in germinal center light or dark zones at 7 days post boost and analyzed by flow cytometry. Light and dark zone: gated on live/single transferred ($CD45.1^+$, inactive PA-GFP+), GC (FAS^{hi}) photoactivated cells. Non-CG B cells, shown for comparison, were identified as FAS- MHC II^+ cells in the small lymphocyte gate.

(B) Larger cells in DZ are undergoing division. Forward scatter (FSC) vs. DNA content (DAPI) among cells photoactivated in LZ or DZ. Gated as in (A). All plots representative of at least 2 independent experiments (pools of 3-5 mice each).

Figure S3. Phenotype of light and dark zone cells from polyclonal primary GCs. Related to Figure4.

(A) Diagrammatic representation of the experimental protocol.

(B) Histograms showing expression of surface markers on LZ and DZ cells gated based on expression of CXCR4 and CD86, as specified and quantified in Figure 4. Non-GC B cells are gated as $B220^+FAS^-CD38^+$.

(C) Sorting strategy for qPCR and post-sort analysis.

(D) Cell cycle analysis of primary GC LZ and DZ cells gated based on expression of CD83 and CXCR4. Bottom-left panel, quantification of data from two indepentent experiments; each symbol represents one mouse. Right panel, cells in G2/M concentrate in the DZ gate. Percentages refer to G2/M cells.

** $p < 0.01$; *** $p < 0.001$; **** $p < 0.0001$, paired T test.

Figure S4. In silico model of transzone migration dynamics of photactivated B cells. Related to Figure 5.

(A) Total number of photoactivated B cells in experiment (squares) and *in silico* (full lines) for DZ to LZ (red) and LZ to DZ (blue) experiments.

(B) Number of photoactivated cells transmigrating from DZ to LZ (red) and from LZ to DZ (blue) determined by experiment (squares) compared to *in silico* results (full lines).

(C) Percentage of photoactivated B cells appearing in the opposite zone in DZ to LZ (red) and LZ to DZ (blue) experiments (squares; mean of data shown in Figure 5D), superimposed onto *in silico* results (full lines).

All experimental data are given as mean with one standard deviation. Note that the first data point in the total number of photoactivated B cells (panel A) is systematically larger *in silico* compared to experiment due to substantial overlap between photoactivated cells at this time point, which leads to underestimation of the experimental value. Otherwise, the *in silico* model and experimental data agree to within one standard deviation.

Figure S5. T cell help limits interzonal migration. Related to Figure 6.

(A) Diagrammatic representation of the experimental protocol for panels B and C.

(B) LZ/DZ distribution and DNA content (DAPI) among transferred B1-8^{hi} (CD45.1^{+}) and endogenous (CD45.1^{-}) GC cells from the same mice (untreated). Right panel, quantification. Each symbol represents one mouse. ** $p < 0.01$; *** $p < 0.001$, paired T test.

(C) Effect of NP-dextran treatment on established GCs. Upper-left: GC size (% FAS^{hi}CD38^{-} cells among B220^{+} cells); upper-right: proportion of B1-8^{hi} and endogenous cells in GC and of endogenous cells among total B cells (in red, left axis); bottom: LZ/DZ ratio and proportion of DAPI high cells among B1-8^{hi} and endogenous populations, at different times after injection of NP-dextran. Representative of two independent experiments, total of 5 mice per group.

(D) Left: DEC205 expression in GC cells from popliteal LNs of DEC205$^{+/+}$ and DEC205$^{-/-}$ mice, 10 days after immunization with NP-OVA-alum. Right: DEC205 expression in LZ (CD86^{hi}CXCR4^{lo}) and DZ (CD86^{lo}CXCR4^{hi}) B cells from DEC205+/+ mice from the same experiment. Both panels representative of two experiments.

(E) Antigen presentation following targeting of GC cells with anti-DEC205. B10.BR mice were immunized with NP-KLH-alum into the hind footpads. On day 10, mice were injected with 3µg of the indicated reagent per footpad and 6 h later popliteal LN were harvested and cells stained with antibody AW3.18 (anti-I-Ek-HEL$_{48-62}$). ISO, isotype control. Graph: each symbol represents one mouse; two independent experiments, two mice per experiment. gMFI, geometric mean fluorescence intensity.

(F) Light/dark zone distribution, DNA content (DAPI), and fraction of DEC205$^{+/+}$ and DEC205$^{-/-}$ GC cells upon treatment with αDEC-CS. Details as in Figure 6. Data are from

two independent experiments. Bottom-left: confocal image showing distribution of DEC205$^{+/+}$ cells in a GC 12h after treatment with αDEC-CS. Colors as in Figure 6.

(G) Light/dark zone distribution and DNA content (DAPI) of DEC205$^{+/+}$ and DEC205$^{-/-}$ GC cells from mice immunized and treated as indicated. Details as in Figure 6. Four mice per timepoint, from at least two independent experiments.

All error bars represent SEM.

Figure S6. T cell help limits germinal center selection and affinity maturation. Related to Figure 7.

(A) Fraction of GC cells derived from transferred DEC205$^{+/+}$ and DEC205$^{-/-}$ B1-8^{hi} and endogenous (DEC205$^{+/+}$) cells in popliteal lymph nodes 72 hours after treatment with αDEC-OVA or αDEC-CS. PA-GFP is used here in its inactive form (405 nm excitation wavelength), as a genetic label for flow cytometry.

(B) Diagrammatic representation of the experimental protocol for Figure 7G.

(C) Diagrammatic representation of the experimental protocol for Figure 7H.

Supplemental Movie Legends

Movie S1. *In vivo* photoactivation. Related to Figure 1. Photoactivation at 830 nm followed by imaging at 940 nm. Green, photoactivated cells; red, transferred (control) dsRed^{+} T cells; blue, collagen (2nd harmonics). Most of the imaging field is occupied by a B cell follicle (note absence of red transferred T cells).

Movie S2. Motility following photoactivation. Related to Figure 1. Collapsed 4D data set showing motility of naïve T cells after photoactivation. Green, photoactivated cells; red, transferred (control) dsRed^{+} cells; blue, collagen (2nd harmonics).

Movie S3. Photoactivation of light and dark zones. Related to Figure 2. Pre and post photoactivation Z-stacks are shown. Light zones were identified by FDC labeling with NP-tdTomato (red); dark zones were identified by presence of autofluorescent tingible-body macrophages (white). Green, photoactivated cells; blue, collagen (2nd harmonics).

Movie S4. Motility following photoactivation. Related to Figure 5. Collapsed 4D data set showing motility of GC B cells at different times after photoactivation in the DZ. Green, photoactivated cells; red, NP-tdTomato (FDC labeling); blue control (CFP+) GC B cells and collagen (2nd harmonics). Early and late movies were taken at different depths in the same GC; therefore FDC distribution within the field of view differs between the two timepoints.

Movie S5. Motility following photoactivation. Related to Figure 5. As in Movie S4, but cells were photoactivated in the LZ.

Supplementary Table Legends

Table S1. Full list of genes differentially expressed by light and dark zone B cells. Related to Figure 3. Includes lists based on 2-fold and 1.33-fold cutoff points (the latter was used for Gene Ontology analysis only).

Table S2. Gene Ontology (GO) analysis of light and dark zone gene expression. Related to Figure 3. Curated list of GO categories (biological process [BP] and cellular compartment [CC]) overrepresented in light zone or dark zone samples in comparison to the entire mouse genome.

Table S3. Gene Set Enrichment Analysis (GSEA) of dark and light zone gene expression. Related to Figure 3. Enrichment scores for selected gene signatures (derived from the literature or from the GSEA c3.tft database) in light zone and dark zone samples.

Table S4. Reagents used for flow cytometry. Related to Figures 2 and 4-7. This table provides a list of all antibodies used for flow cytometry.

Table S5. Primers used for quantitative PCR. Related to Figure 4. This table provides the sequence for primers used for determining gene expression by quantitative RT-PCR.

Extended Experimental Procedures

Cell transfer

Spleens and lymph nodes were forced through a 70 µm mesh into complete RPMI media (Gibco) with 10% serum. Resting B cells and $CD4^+$ T cells were obtained by magnetic cell sorting (MACS) using anti-CD43 beads and the $CD4^+$ T cell isolation kit (Miltenyi), respectively, according to the manufacturer's instructions. $Ig\lambda^+$ B cells were isolated by staining with 0.1 µg/ml phycoerythrin-conjugated anti-Igκ (BD, Clone 187.1) followed by separation with anti-PE and anti-CD43 magnetic beads (Miltenyi).

Immunization

To generate secondary GCs, male B6 recipient mice were immunized intraperitoneally with 50 µg ovalbumin (Sigma) precipitated in alum (Imject® Alum, Thermo Scientific) at 2:1 ratio in a 100 µl volume. Two to four weeks later, mice were boosted with 25 µg of $NP_{(19)}$-OVA (Biosearch Technologies) in each hind footpad. One day prior to boosting, either 5-10x10^6 B1-8^{hi} or 0.5-1.5x10^6 $Ig\lambda^+$ B1-8^{hi} B cells of various genotypes were transferred intravenously, at the ratios indicated in each figure. Popliteal lymph nodes were analyzed 7 or 8 days later, depending on the experiment. For the control experiment in Fig. S5G, mice were immunized with keyhole limpet hemocyanin (KLH, Sigma) and boosted with $NP_{(19)}$-KLH (Biosearch Technologies), following the same protocol. To generate primary, polyclonal GCs, mice were immunized subcutaneously in all four footpads and in the base of the tail with 50 µg $NP_{(19)}$-KLH (Biosearch

Technologies) in alum at 2:1 ratio in a 150 μl volume. Draining lymph nodes (popliteal, inguinal, axilary, brachial) were harvested 10 days later for analysis. For ELISA experiments, OVA-immunized mice were boosted subcutaneously 2-4 weeks after immunization with 100 μg $NP_{(3)}$-OVA (see below). For sequencing of primary GCs, mice were immunized intraperitoneally with $NP_{(19)}$-OVA precipitated in alum.

Photoactivation

Conditions for photoactivation differed according to purpose and imaging conditions in each experiment. For flow cytometry or cell sorting experiments, large 3D areas of LZ or DZ were photoactivated by a single, higher-power scan using 830 nm wavelength and 5 μm Z resolution. Transitional areas less than 10 μm (2 Z slices) away from the LZ/DZ border were avoided. For intravital tracking experiments, smaller areas of LZ or DZ were photoactivated by multiple (2-4) lower-power scans repeated at 4-second intervals. This protocol was optimal for achieving maximal contrast with minimal photodamage. Cell motility was monitored immediately after activation and at later time points as a measure of survival, and experiments in which motility was altered following photoactivation were discarded. All imaging experiments were carried out using either an Olympus BX61 upright microscope (Olympus 25X 1.05 NA Plan objective), fitted with a Coherent Cameleon Vision II laser (live mouse experiments) or a Zeiss LSM710 NLO inverted microscope (Zeiss 25X 0.8 NA Plan objective) with a SpectraPhysics MaiTai DeepSee laser (flow cytometry experiments).

FDC labeling

Red fluorescent protein tdTomato (Shaner et al., 2004) was produced in *E. coli* as a GST fusion protein and purified using Glutathione Sepharose^{TM} beads (4 Fast Flow, GE Healthcare). tdTomato was then conjugated with 4-hydroxy-3-nitrophenylacetyl (NP) succinimidyl ester (Biosearch Technologies) to a hapten-to-protein ratio of ~11. Lipopolysaccharide and other contaminants were removed from the preparation using Triton X-114 as described (Aida and Pabst, 1990), and residual detergent was removed by centrifugation through a 30 kDa Centricon (Millipore). For FDC labeling, mice were injected subcutaneously with 2 µg per hind footpad of NP-tdTomato one day prior to imaging. For PE IC labeling, mice received an intravenous injection of 2 mg polyclonal rabbit anti B-PE (Rockland) followed by a subcutaneous injection of 2 µg per hind footpad of B-PE (Invitrogen) 1 day before imaging (Allen et al., 2007).

Sample preparation for intravital imaging

Mice were anaesthetized with 100 mg ketamine, 15 mg xylazine and 2.5 mg acepromazine per kg body weight and were kept anaesthetized by inhalation of 1.25% isofluorane in 100% oxygen for up to 10 hours. The hind legs of mice were shaved using a double-edged razor blade. Mice were restrained on a stage warmer at 37 °C (BioTherm Micro S37; Biogenics) and an incision was made behind the knee of one hind leg. The connective and adipose tissue covering the lymph node were aseptically removed by microsurgery while maintaining blood and lymph vessels intact. The lymph node and leg were then held in position using a metal strap fixed to the stage warmer,

with a small opening through which the node was imaged. For long time courses, mice were kept hydrated by regular injections of lactated Ringer's solution.

Image acquisition

All images presented were acquired on the Olympus system, using 940 nm excitation and the following filters: a first pair of overlapping CFP (460-510) and GFP (495-540) filters, separated by a 505 dichroic mirror, which allowed maximal signal detection for both PA-GFP and CFP; second harmonics (collagen) was also detected in the CFP filter at 940 nm excitation; and a third filter (575-630) for the red signal (tdTomato or phycoerythrin). For time series, we typically acquired 250 µm-deep Z-stacks with 5 µm Z resolution, with an X-Y resolution of 800 x 800 pixels and ~0.5-0.8 µm per pixel. Movies were taken at lower resolution and different volumes were imaged according to purpose and imaging conditions. Z resolution was always 5 µm and time resolution ranged from 20 s to 64 s per frame.

Image analysis

Prior to data analysis, the PA-GFP signal was separated from autofluorescence and bleedthrough from CFP using the colocalization option in Imaris software v.6.4.0 (Bitplane). The position of photoactivated cells was determined manually, slice by slice, by combining the *Spots* and *Ortho-slicer* tools in Imaris. Cells photoactivated in the DZ were considered as having transitioned to the LZ when positioned within the area of

bright NP-tdTomato staining (above the transitional area of weak antigen retention). Conversely, cells photoactivated in the LZ were considered as being having transitioned to the DZ when positioned within areas of very week or absent NP-tdTomato staining but still within the GC dark zone (as indicated by presence of CFP cells and tingible body macrophages). In both cases, cells in the transitional area of weak antigen retention were considered as remaining in their zone of origin. *Movie analysis:* Cells were tracked manually in 4 dimensions using the *Track cells manually* tool in Volocity software v. 5.0 (Perkin-Elmer). All photoactivated PA-GFP cells and a similar number of control cells were tracked. In case of excess of control cells, a sample of these cells was selected by determining a region of interest and tracking all cells whose tracks started within that region. Mean cell speed was calculated automatically in Volocity. Both static and dynamic movies were annotated and edited for presentation using ImageJ (NIH), Adobe Photoshop and Adobe After Effects.

Flow cytometry and cell sorting

Lymph nodes were forced through a 70 µm mesh into complete RPMI with 10% fetal calf serum. Single-cell suspensions thus obtained were pretreated for 5' with 1 µg/ml of anti-CD16/32 (24G2, eBioscience) and then stained for 30 min at 4^{o}C in PBS supplemented with 2% FCS and 1mM EDTA using the reagents listed in Table S4. For cell cycle analysis, cells were fixed and permeabilized using the Cytofix/Cytoperm^{TM} kit (BD) and stained with 10 µg/ml DAPI (Invitrogen) for 5 minutes. Samples were analyzed on an LSR-II flow cytometer (BD). Unless otherwise indicated, GC cells were gated as

live/single, $B220^+$ or $CD19^+$, FAS^{hi}, and $CD38^-$ and/or $GL\text{-}7^+$. For cell sorting, cells were stained as above and sorted directly into Trizol® or Trizol LS® reagent (Invitrogen) using a FACS Aria (Benton Dickinson) at the Nussenzweig lab or at the Rockefeller University Flow Cytometry Resource Center. Cells were maintained at 4^oC at all times.

Microarray analysis

Raw data were normalized using the RMA algorithm in GeneSpring v. 11 software (for dot plots and heatmaps) or using the ExpressionFileCreator module from GenePattern for GSEA analysis (Reich et al., 2006). Genes used to estimate the magnitude of the difference between LZ and DZ gene expression and for generating the heatmaps in Figure 3B differed by at least 2-fold in both replicate analyses (LZ[A]≠DZ[A], LZ[B]≠DZ[B]) at $p<0.2$. Gene ontology analysis was carried out using DAVID Bioinformatics Resources v.6.6 (CC_FAT and BP_FAT) (Dennis et al., 2003; Huang da et al., 2009). The expanded gene set used for this analysis included all genes differing between LZ and DZ at $p<0.05$ plus all genes differing by at least 1.33-fold in the four possible comparisons between both replicate analyses (LZ[A]≠DZ[A], LZ[A]≠DZ[B], LZ[B]≠DZ[A], LZ[B]≠DZ[B]) at $p<0.2$. Both sets are included in Table S1. GSEA analysis was carried out using GSEA software v.2.0 (Mootha et al., 2003; Subramanian et al., 2005) LZ/DZ array data was ranked using the log2_Ratio_of_Classes metric. Foreground lists included the Broad Institute c3.tft predicted transcription-factor binding motif sets (Xie et al., 2005) and gene signatures from Basso et al., 2004 and Zhu et al,. 2004.

NP conjugation

4-hydroxy-3-nitrophenylacetyl (NP) succinimidyl ester (Biosearch Technologies, Novato, CA) was conjugated to ovalbumin (Sigma), 70 kDa amino dextran (Invitrogen), and αDEC205-CS in our laboratory, at hapten-to-macromolecule ratios of ~3, ~24, and ~6, respectively.

ELISA

High- and low-affinity NP-specific antibodies were measured by ELISA with $NP_{(3)}$-BSA and $NP_{(23)}$-BSA (Biosearch Technologies) as the coating reagent, respectively. NP-specific IgG_1 was detected using goat anti–mouse IgG_1 Fc-specific antibody conjugated to horseradish peroxidase (Jackson ImmunoResearch) followed by the 1-Step ABTS kit (Pierce). OD405 was measured using a VERSAmax microplate reader (Molecular Devices). Titers represent the highest serum dilution showing an OD405 >0.1. Samples with titers lower than 100 were set to 100.

PCR and sequence analysis

Genomic DNA was extracted from sorted GC cells and nested PCR was used to amplify VH186.2-JH2 genes. Clones were amplified using the outer primers 5′-CATGGGATGGAGCTGTATCATGC-3′ (forward) and 5′-CTCACAAGAGTCCGATAGACCCTG-3′ (reverse) for 25 cycles at 94°C for 30 s, 55.5°C for 30 s, and 72°C for 90 s, followed by the inner primers 5′-GGTGACAATGACATCCACTTTGC-3′ (forward) and 5′-GACTGTGAGAGTGGTGCCTTG-3′ (reverse) using the same conditions. PCR was performed with DNA from approximately 4 thousand GC cells (25 ng) per reaction, using high-fidelity Pfu DNA polymerase (Stratagene). Amplified products were cloned (Topo Cloning kit; Invitrogen), sequenced, and analyzed using MacVector 11.1. We analyzed only clones bearing a V186.2 segment (V1-72*01), as determined using the IMGT/V-QUEST system (Brochet et al., 2008).

Immunofluorescence and confocal microscopy

Cryostat sections of lymph nodes were fixed and stained as described previously (Lindquist et al., 2004). Sections were stained using the following reagents: anti-CD35-biotin (clone 8c12, BD), anti-GFP-Alexa 488 (rabbit polyclonal IgG, Invitrogen), anti-IgD (clone 11.26, BD), conjugated to Alexa 647 in our laboratory, and Streptavidin-Cy3 (Jackson ImmunoResearch). Confocal images were acquired on a Zeiss LSM 510 system with 488-, 543- and 633-nm excitation line (Rockefeller University Bio-Imaging Facility). Images were obtained with a Plan-Apochromat 20X (NA 0.75) objective. Images were exported to Adobe Photoshop CS4 for final processing.

Half-life determination:

PA-GFP$^{+/+}$CD45.1$^{+/+}$ splenic B cells were photoactivated *ex vivo* using a 415 nm LED light source (Prizmatix) for 10 minutes and then transferred into wild-type recipient mice, which were sacrificed 24 or 48 h after transfer. Transferred cells were identified by flow cytometry by expression of CD45.1. The fluorescence of photoactivated PA-GFP was calculated as gMFI (488 nm) photoactivated cells – gMFI (488 nm) non-photoactivated cells. Half-life was calculated using the *one phase exponential decay* function in Prism software v. 5.0 (Graphpad).

Mathematical model for GC B cell dynamics

The aim of this modeling approach was to derive the fraction of B cells in the LZ that is selected and return to the DZ for proliferation from the measured interzonal migration events observed in photoactivated cells. Let us denote photoactivated GC B cells in the DZ with *B* and in the LZ with *C*. In the spirit of a cyclic re-entry model we chose:

$$\begin{aligned} \frac{dB}{dt} &= pB - mB + m'C \\ \frac{dC}{dt} &= mB - m'C - \gamma C \end{aligned}$$

where *m* and *m'* are the transition rates (per time) from DZ to LZ and LZ to DZ, respectively. *p* is the proliferation rate and *γ* is the amount of cell loss due to emigration and cell death or other processes.

The equations are solved numerically to reproduce the time dynamics of interzonal migration events as found in experiment. The initial condition is set to the average maximum value of B cells observed in experiment. As proliferation is a slow process when compared to the duration of the experiments, we chose p=0. The result is compared to the mean values of all experiments at any time point. The fraction of LZ B cells that get selected and return to the DZ in this model was calculated as $F = m'C/(\gamma C+m'C) = m'/(\gamma+m')$.

Supplementary References

Aida, Y., and Pabst, M.J. (1990). Removal of endotoxin from protein solutions by phase separation using Triton X-114. J Immunol Methods *132*, 191-195.

Allen, C.D., Okada, T., Tang, H.L., and Cyster, J.G. (2007). Imaging of germinal center selection events during affinity maturation. Science *315*, 528-531.

Brochet, X., Lefranc, M.P., and Giudicelli, V. (2008). IMGT/V-QUEST: the highly customized and integrated system for IG and TR standardized V-J and V-D-J sequence analysis. Nucleic Acids Res *36*, W503-508.

Dennis, G., Jr., Sherman, B.T., Hosack, D.A., Yang, J., Gao, W., Lane, H.C., and Lempicki, R.A. (2003). DAVID: Database for Annotation, Visualization, and Integrated Discovery. Genome Biol *4*, P3.

Huang da, W., Sherman, B.T., and Lempicki, R.A. (2009). Systematic and integrative analysis of large gene lists using DAVID bioinformatics resources. Nat Protoc *4*, 44-57.

Lindquist, R.L., Shakhar, G., Dudziak, D., Wardemann, H., Eisenreich, T., Dustin, M.L., and Nussenzweig, M.C. (2004). Visualizing dendritic cell networks in vivo. Nat Immunol *5*, 1243-1250.

Mootha, V.K., Lindgren, C.M., Eriksson, K.F., Subramanian, A., Sihag, S., Lehar, J., Puigserver, P., Carlsson, E., Ridderstrale, M., Laurila, E.*, et al.* (2003). PGC-1alpha-responsive genes involved in oxidative phosphorylation are coordinately downregulated in human diabetes. Nat Genet *34*, 267-273.

Reich, M., Liefeld, T., Gould, J., Lerner, J., Tamayo, P., and Mesirov, J.P. (2006). GenePattern 2.0. Nat Genet *38*, 500-501.

Shaner, N.C., Campbell, R.E., Steinbach, P.A., Giepmans, B.N., Palmer, A.E., and Tsien, R.Y. (2004). Improved monomeric red, orange and yellow fluorescent proteins derived from Discosoma sp. red fluorescent protein. Nat Biotechnol *22*, 1567-1572.

Subramanian, A., Tamayo, P., Mootha, V.K., Mukherjee, S., Ebert, B.L., Gillette, M.A., Paulovich, A., Pomeroy, S.L., Golub, T.R., Lander, E.S.*, et al.* (2005). Gene set enrichment analysis: a knowledge-based approach for interpreting genome-wide expression profiles. Proc Natl Acad Sci U S A *102*, 15545-15550.

Xie, X., Lu, J., Kulbokas, E.J., Golub, T.R., Mootha, V., Lindblad-Toh, K., Lander, E.S., and Kellis, M. (2005). Systematic discovery of regulatory motifs in human promoters and 3' UTRs by comparison of several mammals. Nature *434*, 338-345.

Supplemental Figure 1

Figure S1

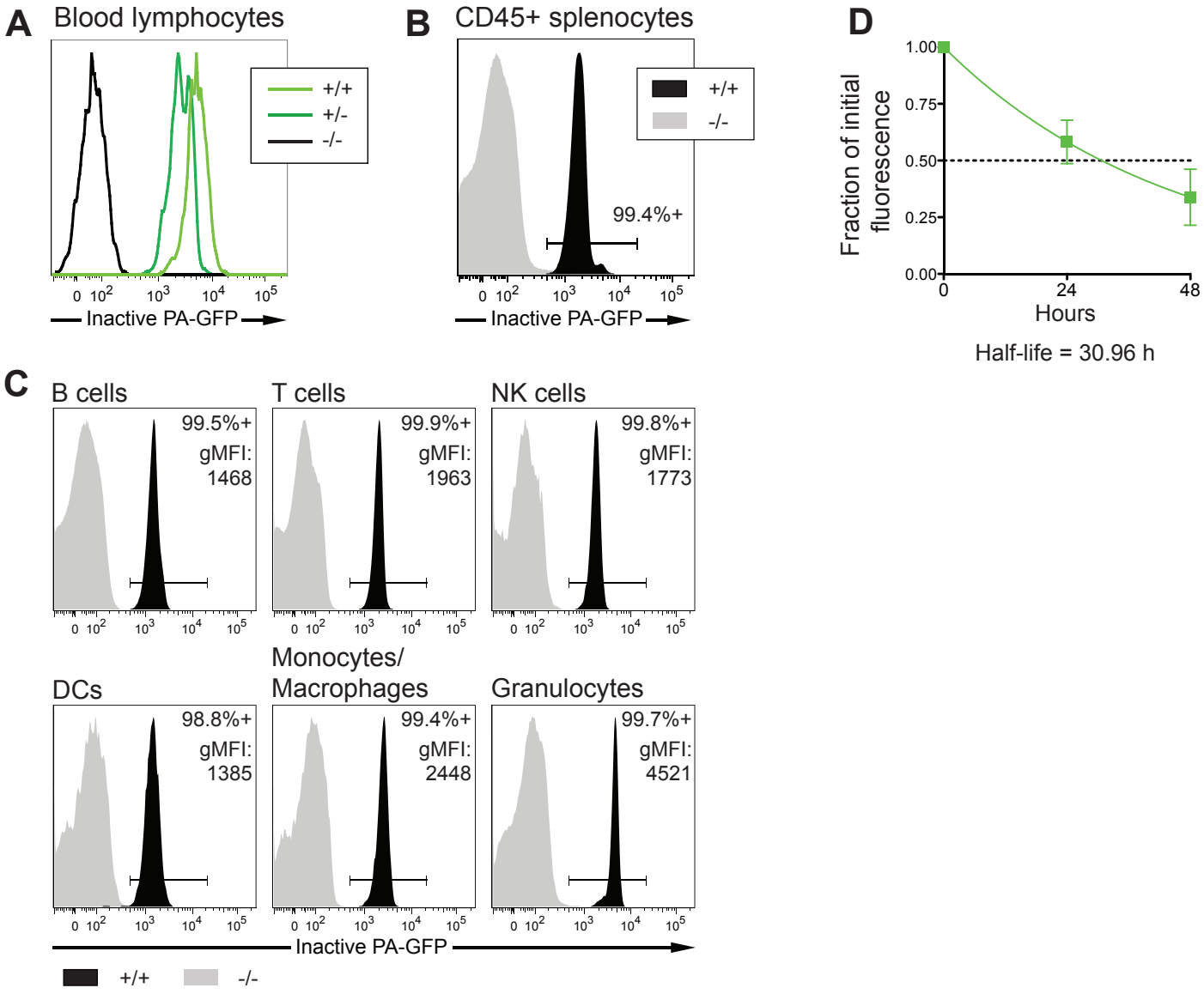

Supplemental Figure 2

Figure S2

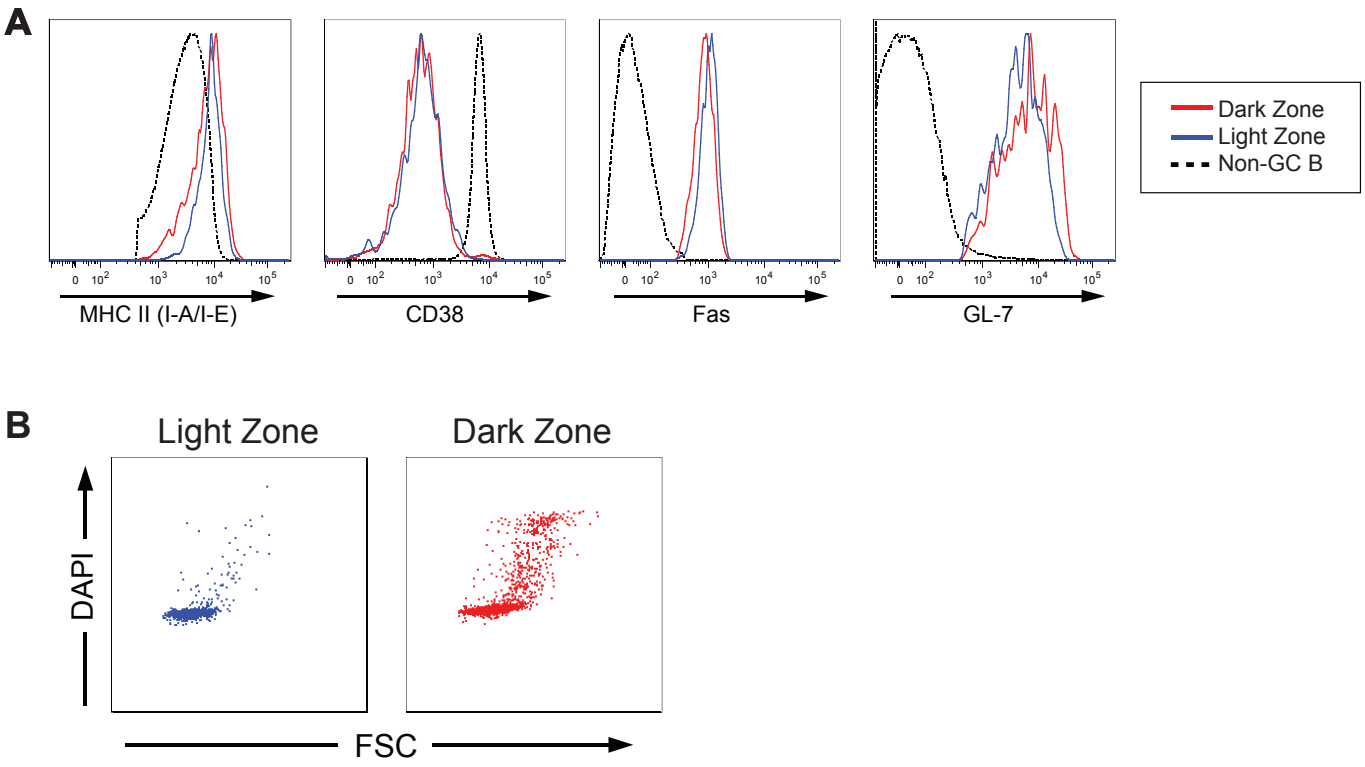

Supplemental Figure 3

Figure S3

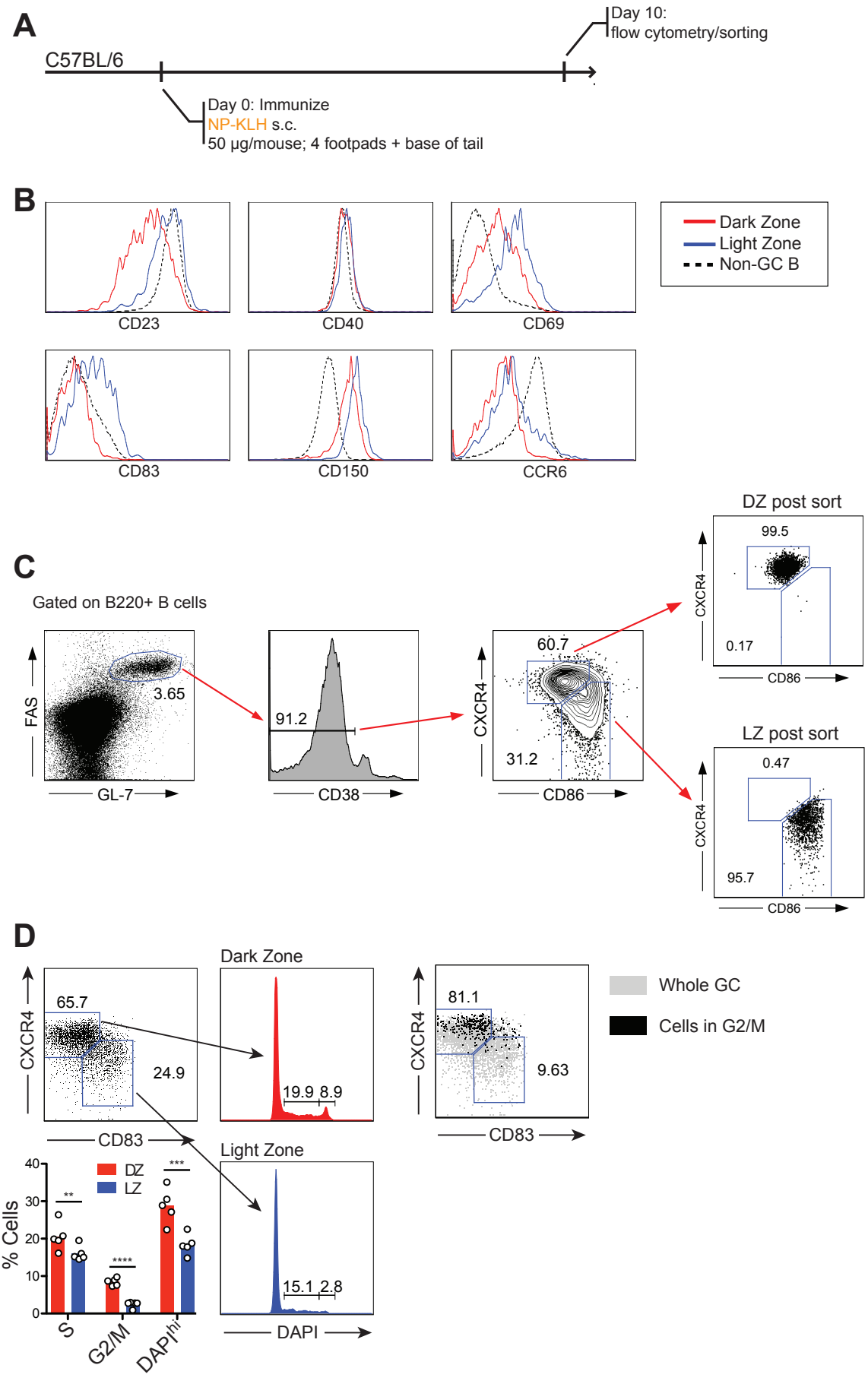

Supplemental Figure 4

Figure S4

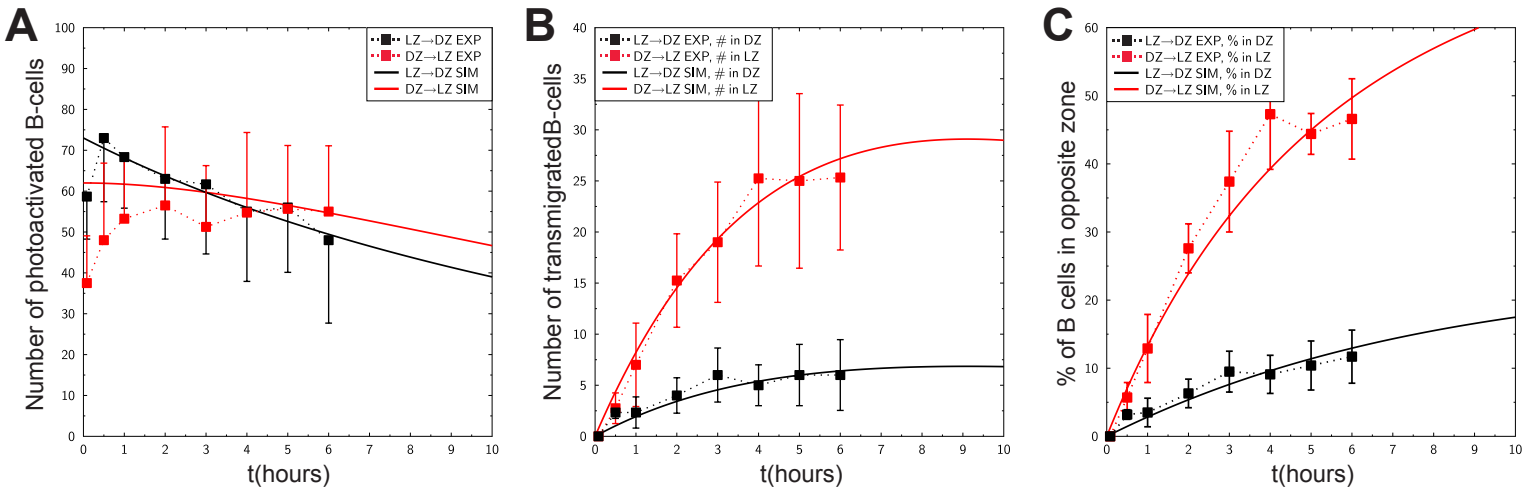

Supplemental Figure 5

Figure S5

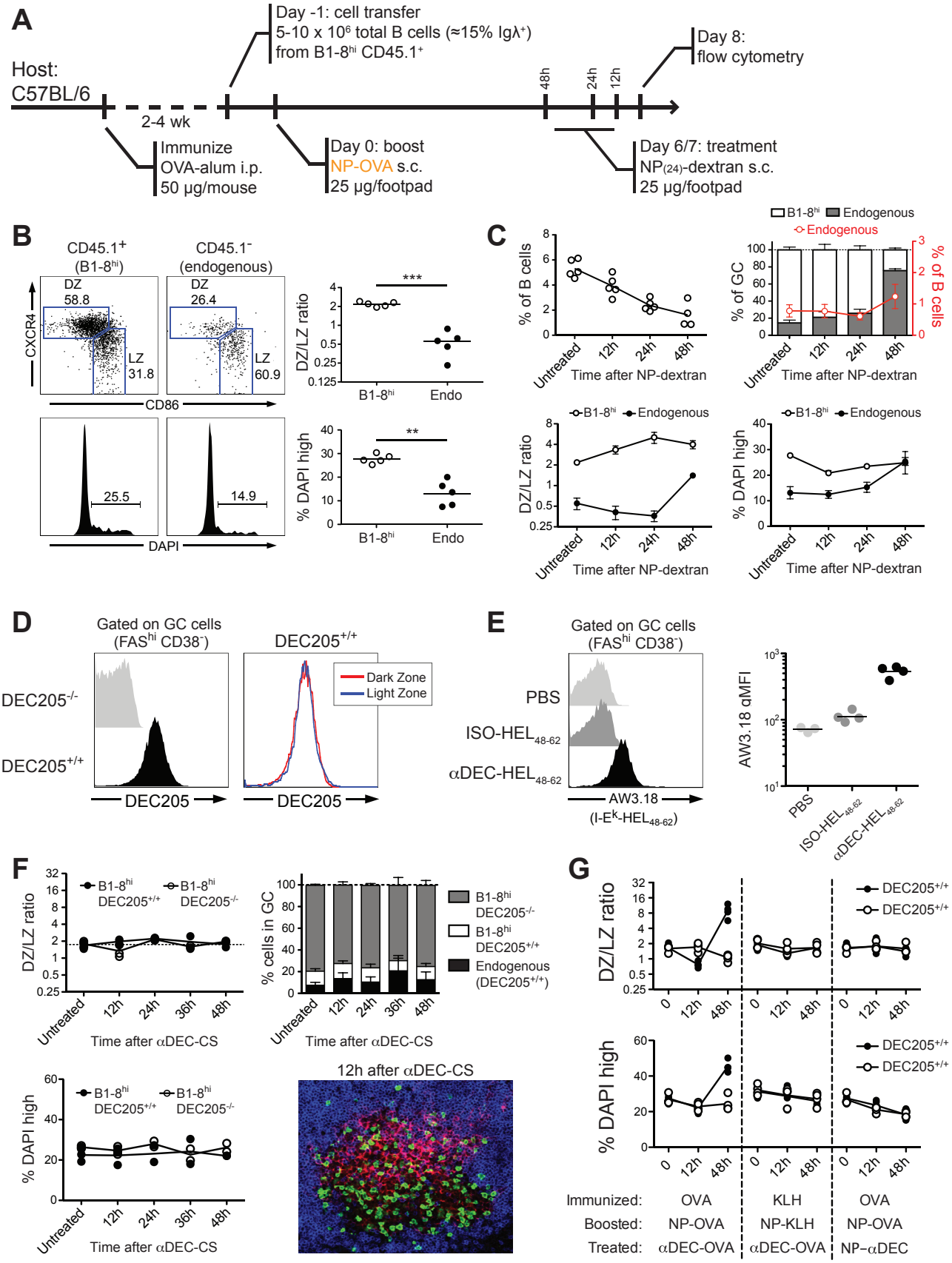

Supplemental Figure 6

Figure S6